Chemistry & Biology
Article

A Chemical Genomic Approach Identifies Matrix Metalloproteinases as Playing an Essential and Specific Role in *Xenopus* Melanophore Migration

Matthew L. Tomlinson,[1] Pingping Guan,[2] Richard J. Morris,[2] Mark D. Fidock,[3] Martin Rejzek,[4] Carla Garcia-Morales,[1] Robert A. Field,[4] and Grant N. Wheeler[1,*]
[1]School of Biological Sciences, University of East Anglia, Norwich, NR4 7TJ, UK
[2]Department of Computational and Systems Biology, The John Innes Centre, Norwich, NR4 7UH, UK
[3]Discovery Biology, Pfizer, Sandwich, Kent, CT13 9NJ, UK
[4]Department of Biological Chemistry, The John Innes Centre, Norwich, NR4 7UH, UK
*Correspondence: grant.wheeler@uea.ac.uk
DOI 10.1016/j.chembiol.2008.12.005

SUMMARY

To dissect the function of matrix metalloproteinases (MMPs) involved in cellular migration in vivo, we undertook both a forward chemical genomic screen and a functional approach to discover modulators of melanophore (pigment cell) migration in *Xenopus laevis*. We identified the 8-quinolinol derivative NSC 84093 as affecting melanophore migration in the developing embryo and have shown it to act as a MMP inhibitor. Potential targets of NSC 84093 investigated include MMP-14 and MMP-2. MMP-14 is expressed in migrating neural crest cells from which melanophores are derived. MMP-2 is expressed at the relevant time of development and in a pattern that suggests it contributes to melanophore migration. Morpholino-mediated knockdown of both MMPs demonstrates they play a key role in melanophore migration and partially phenocopy the effect of NSC 84093.

INTRODUCTION

Over the last 10 years, chemical genomics has received a lot of interest from the chemical biology community (Schreiber, 1998; Spring, 2005). With the aid of appropriate high-throughput synthesis and well-defined biological screening strategies, it is feasible to identify specific small molecule inhibitors of many biological events (Adams and Levin, 2006; Ding and Schultz, 2004; Stockwell, 2000). The approach provides fundamental challenges for synthetic and analytical chemistry on the one hand, and novel opportunities to manipulate biological systems on the other (Ansari, 2007; Knight and Shokat, 2007; Schreiber, 1998; Yeh and Crews, 2003).

Small molecule intervention offers a complimentary approach to loss-of-function mutations in the analysis of complex, multicomponent biological processes such as cell signaling and morphogenesis. Whole animal high-throughput chemical genomic screens have been developed for *Drosophila*, *Caenorhabditis elegans*, zebrafish, and *Xenopus* (Carroll et al., 2003; Kwok et al., 2006; Tomlinson et al., 2005; Zon and Peterson, 2005). An advantage of chemical genomic screens over mutagenesis screens is that they allow for temporal control of protein function.

With respect to vertebrate development, the number of compounds so far identified with specific developmental effects is small. Such compounds often come from natural sources, as in the case of cyclopamine, which blocks the hedgehog pathway (Cooper et al., 1998). The recent use of zebrafish (Zon and Peterson, 2005) and *Xenopus* (Fukumoto et al., 2005; Tomlinson et al., 2005) in chemical genomic screening has opened up new opportunities. To date, chemical genomic screens have identified compounds that modulate embryonic development (Anderson et al., 2007; Burns et al., 2005; Fukumoto et al., 2005; Kwok et al., 2006; Mathew et al., 2007; Peterson et al., 2000; Singh et al., 2005; Tomlinson et al., 2005; Yu et al., 2008) and help with drug target discovery (Adams and Levin, 2006; Langheinrich et al., 2002; Lunn and Stockwell, 2005), target validation, and toxicological studies (Langheinrich, 2003; Peterson et al., 2001). Chemical genomics is also becoming increasingly important in identifying new molecular tools for studying developmental processes. Recent advances include the use of a compound (MoTP) to specifically ablate embryonic melanophores (Yang and Johnson, 2006). This allowed the important discovery of melanophore stem cell populations in developing zebrafish embryos (Yang et al., 2007; Yang and Johnson, 2006).

The study presented here focused on melanophores as an in vivo model for cellular migration. The main function of melanophores (melanocytes in higher vertebrates) is pigment production, which aids camouflage (and thus reduces predation) and protects the skin from deleterious agents such as free radicals and ultraviolet irradiation (UV) (Lamason et al., 2005; Riley, 1997). In the developing *Xenopus* embryo, as in all vertebrates, the melanophores arise as melanoblasts from a pluripotent neural crest cell (NCC) population on the dorsal side of the neural tube (Le Douarin and Dupin, 2003). Melanoblasts are potentially specified to become melanophores before migration as shown by XIDCT expression (Kumasaka et al., 2003; see Figure S2 available online). They then actively migrate extensive distances to form two distinctive pigment stripes in the embryo, the lateral and dorsal stripes (Collazo et al., 1993; Kumasaka et al., 2003); see Figures 1A and 1C). The lateral pigment stripe consists of

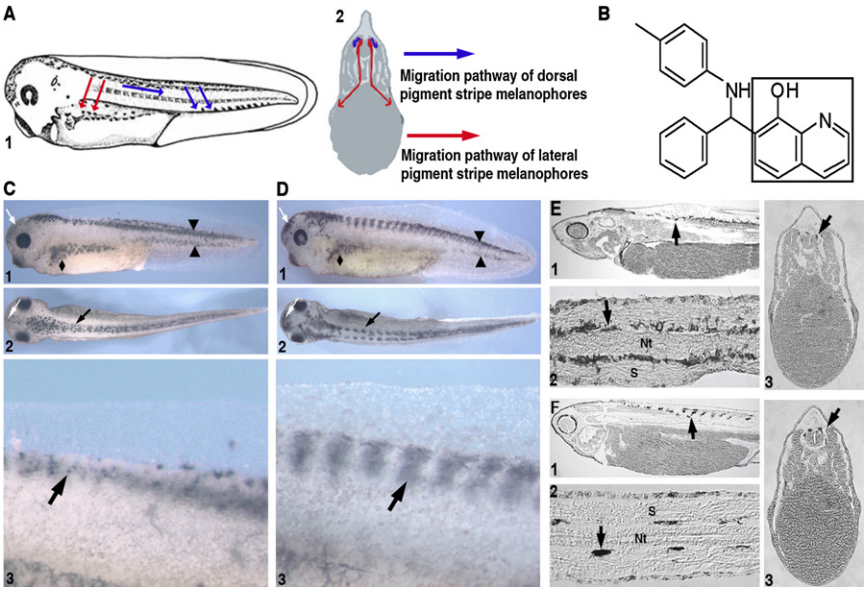

Figure 1. Pigmentation Pattern Seen with Wild-Type and NSC 84093-Treated Embryos

(A) Schematic representation of the migratory pathways taken by the lateral pigment (red arrow) and dorsal pigment (blue arrow) stripe melanophores of a stage 38 wild-type embryo. A1 shows the lateral side of the embryo, whereas A2 shows a transverse view.

(B) Structure of NSC 84093 (7-[(S)-[(4-methylphenyl)amino](phenyl)methyl]quinolin-8-ol) with the quinoline moiety highlighted by the box.

(C) Normal pigmentation patterns seen in wild-type embryos at stage 38 (1–3). C3 shows a close up of the dorsal trunk section of C1.

(D) Disrupted pigmentation pattern seen with the application of 1 μM NSC 84093, showing that the treated embryos lack pigment cells in the ventral part of the dorsal pigment stripe (1–3). D3 shows a close up of the dorsal trunk section of D1 (same position as for C3).

(E and F) Sections showing internal melanophore localization of stage 38 embryos. E1 is a sagittal section with the anterior half of the embryo shown, E2 is a longitudinal section cut at the level of the neural tube, and E3 is a transverse section, midway on the anterior-posterior axis. F 1, 2, and 3 are sections of NSC 84093-treated (1 μM) embryos in the same plane and orientation as for E 1, 2, and 3. Diamond (◆) represents the lateral pigment stripe, and arrowhead (▲) represents the melanophores of the dorsal pigment stripe on the dorsal side of the tail and those that have migrated to the ventral side of the tail. Black arrows show the position of individual melanophores, and white arrows show the position of the pineal body. s represents somites; Nt, neural tube; No, notochord. All embryos are shown in lateral view, with anterior to the left, except C2 and D2, which are dorsal views.

a triangular-shaped patch of melanophores, on both sides of the embryo trunk (Collazo et al., 1993). The dorsal stripe forms a continuous band circumnavigating the embryo tail. Melanophore migration is initiated between stage 24 and 30 in a progressive anterior to posterior wave (Kumasaka et al., 2003). The migration route in respect to the internal structures of the embryo is between the somites and the neural tube, for both pigment stripes (Collazo et al., 1993). Importantly melanophores have also been tracked migrating 2–6 somite lengths in a caudal direction (Collazo et al., 1993; Krotoski et al., 1988).

The study of melanophore migration has potential implications for human health. Melanomas, which originate from melanocytes in the skin, are one of the most dangerous forms of skin cancer because they are highly invasive and resistant to treatment. Human melanomas are known to express a number of matrix metalloproteinases (MMPs), including MMP-14 and MMP-2 (Hofmann et al., 2000). The role of MMP-14 and MMP-2 in melanoma progression is consistent with other cancers, where their expression levels correlate with increased progression and invasiveness, and hence metastasis (Hofmann et al., 2000). The known model of MMP-14/TIMP-2 activation of MMP-2 is also present in metastatic melanoma (Hofmann et al., 2000). The ability to block melanophore migration can be considered a starting point for therapeutic intervention in the treatment of metastatic melanoma (Haass et al., 2005). It is now increasingly recognized that cell motility and invasion could provide a rich source of novel targets for cancer therapy, and that appropriate inhibitors might prevent both metastasis and neoangiogenesis (Eccles et al., 2005). Therefore, one of the possible outputs of chemical genomic studies on melanophore migration might be the identification of novel anticancer lead compounds.

In this study, we identify a small molecule compound (NSC 84093) that selectively inhibits the migration of *Xenopus* melanophores. We characterized this compound further and found that it has the ability to act as a putative MMP inhibitor. We further show that morpholino (MO)-mediated knockdown of *Xenopus* MMP-2 and MMP-14 can partially phenocopy the addition of NSC 84093 and inhibit melanophore migration. We conclude that MMPs are crucial for melanophore migration in vivo.

RESULTS

NSC 84093 Prevents Melanophore Migration by the Dorsal Pathway

We have performed a developmental chemical genomic screen of 3000 compounds (Tomlinson et al., 2009) to identify phenotypes associated with pigment cell development. We have identified 40 compounds, producing varying phenotypes. Compound NSC 84093 (Figure 1B) gave a dramatic pigmentation phenotype (shown in Figure 1D) when applied to the embryos at as little as 1 μM concentration (see Figure S1 for a dose-response curve). The continuous dorsal pigment stripe seen in wild-type embryos (Figures 1C and 1E) failed to form. Instead, in NSC 84093-treated embryos, a segmented pattern of pigment could be seen along the dorsal side of the embryo (Figures 1D and 1F). The ventral side of the tail also lacked the majority of melanophores (Figure 1, D1, indicated by the triangle symbol). The lateral pigment stripe was present and the melanophores from the pineal body in the head migrated normally (Figure 1, D1, indicated by the diamond and the white arrows). The melanophores moved from the dorsal side of the neural tube to be situated on either side (Figure 1, D2). Closer inspection of the segmented dorsal pigment stripe in the treated embryos showed

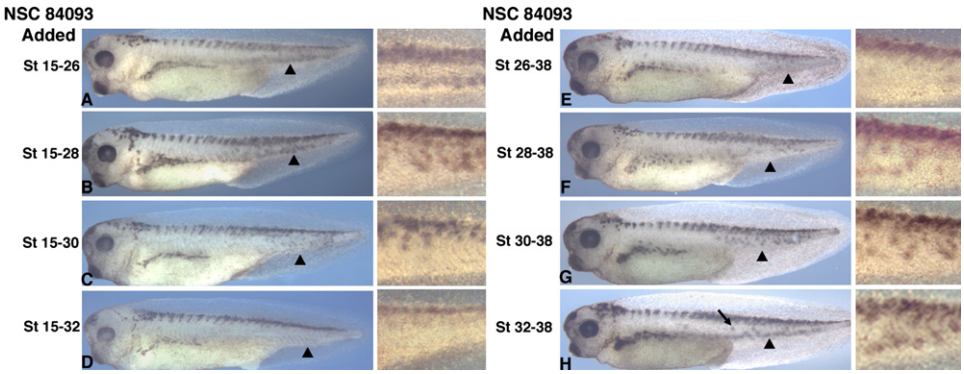

Figure 2. Application and Release Experiments to Dissect the Developmental Window of NSC 84093's Molecular Target
(A–D) Application of NSC 84093 (1 μM) at stage 15 and subsequent release at stage 26 (A), 28 (B), 30 (C), and 32 (D).
(E–H) Application of NSC 84093 (1 μM) at stage 26 (E), 28 (F), 30 (G), and 32 (H). Black arrow shows migrating melanophores. The additional box for each embryo shows a close up of the dorsal stripe in the tail region. 5 represents the dorsal pigment stripe. All embryos are shown in lateral view, with anterior to the left.

that the melanophores are constrained to clearly defined boundaries, giving a sharply segmented appearance (Figure 1, D3). Sections clearly showed that the melanophores were able to migrate between the somites and the neural tube, but failed to migrate any further (Figures 1E and 1F).

NSC 84093 Exerts Its Effect at an Early Point in Migration

To determine the developmental window in which NSC 84093 acts, we applied the compound at different stages of development (Figures 2A–2H). Melanoblasts begin to migrate away from the neural tube around stage 26 (Collazo et al., 1993). We applied the compound before migration started at stage 15 and then removed it at various time points. Applying the compound from stage 15 to 24 did not give a phenotype (data not shown). Applying the compound from stage 15 to 26 showed that NSC 84093 causes the segmented pattern in the anterior dorsal trunk region (Figure 2A). However, the migration of pigment cells to the ventral side of the tail was unperturbed (Figure 2A). Applying the compound at stage 15 to stages 28, 30, and 32 (Figures 2B–2D) showed an increasing inhibition of pigment cell migration to the ventral side of the tail. When the compound was added at stage 26 to 38, the segmentation and a loss of pigment cells in the ventral tail region was seen (Figure 2E). This effect on ventral tail melanophore migration is lessened when the compound is applied at later stages (and left to stage 38) (Figures 2E–2H). The segmented pattern in the anterior dorsal region of the trunk was still observed. These results suggested that a developmental time window between stages 26 and 32 is critical for the molecular action of NSC 84093, with respect to melanophore migration to the ventral side of the tail. These results were confirmed when the compound was applied at stage 26 and removed at stage 32. This caused the same phenotype as that shown in Figure 2D (data not shown).

Using the specific molecular marker *XIDCT* (Kumasaka et al., 2003), we investigated the segmented phenotype further by visualizing the location of melanoblasts on the dorsal side of the neural tube. In the wild-type embryo, at stage 26, the *XIDCT*-expressing cells are randomly distributed, but have not begun migrating (Figure S2, A1 and A2). In the treated embryos, however, a segmented pattern formed and discrete blocks of cells were evident (Figure S2, D1 and D2). At slightly later stages the *XIDCT*+ cells had migrated ventrally in the treated embryos (Figures S2E and S2F compared with S2B and S2C) and formed the distinctive segmented pattern seen in the treated embryos at later stages (Figure 1D).

Effect of NSC 84093 on the Migration of Other NCC-Derived Cells

To investigate if NSC 84093 affected the migration of other NCC derived cells, we looked at the anterior cranial NCC, the iridophores, and the dorsal root ganglion. Cranial NCC migration at stages 22 to 32 was unaffected, as assayed by in situ hybridization using the molecular marker *SOX-10,* though interestingly some segmentation of the SOX-10 pattern can be seen in the trunk (Figures 3A and 3B) (Honore et al., 2003). Iridophores appear iridescent silver to gold by reflecting light, and they can be seen in their postmigration position on the embryos developing intestine in both wild-type and NSC 84093-treated embryos The NSC 84093-treated embryos clearly show the lack of melanophores in the ventral tail region (Figure 3, C1 and C2). Dorsal root ganglion (DRG) cells, which are derived from the trunk neural crest, were marked by antibody staining with β-tubulin III (Lin et al., 2007). Stained embryos were sectioned to reveal the position of the DRG. In both treated and control embryos, the DRG are in their normal position between the somites and the neural tube (Figure 3, D1 and D2).

NSC 84093 Has the Pharmacological Properties of an MMP Inhibitor

We performed structure activity relationship (SAR) analysis on a number of other compounds shown to be similar to NSC 84093 by their pairwise Tanimoto scores. Most of these compounds showed a similar phenotype to NSC 84093, except for NSC 1013 (Figure 4, A1–A6). All of them contain a quinoline scaffold (Figure 1 B, boxed area), suggesting that they have potential affinity for metal ions (Hruby et al., 2004). However, quinolin-8-ol itself had no effect on melanophore migration (Figure 4, A7). To further investigate whether NSC 84093 activity is dependent upon metal ions, we added various cations to see if they could

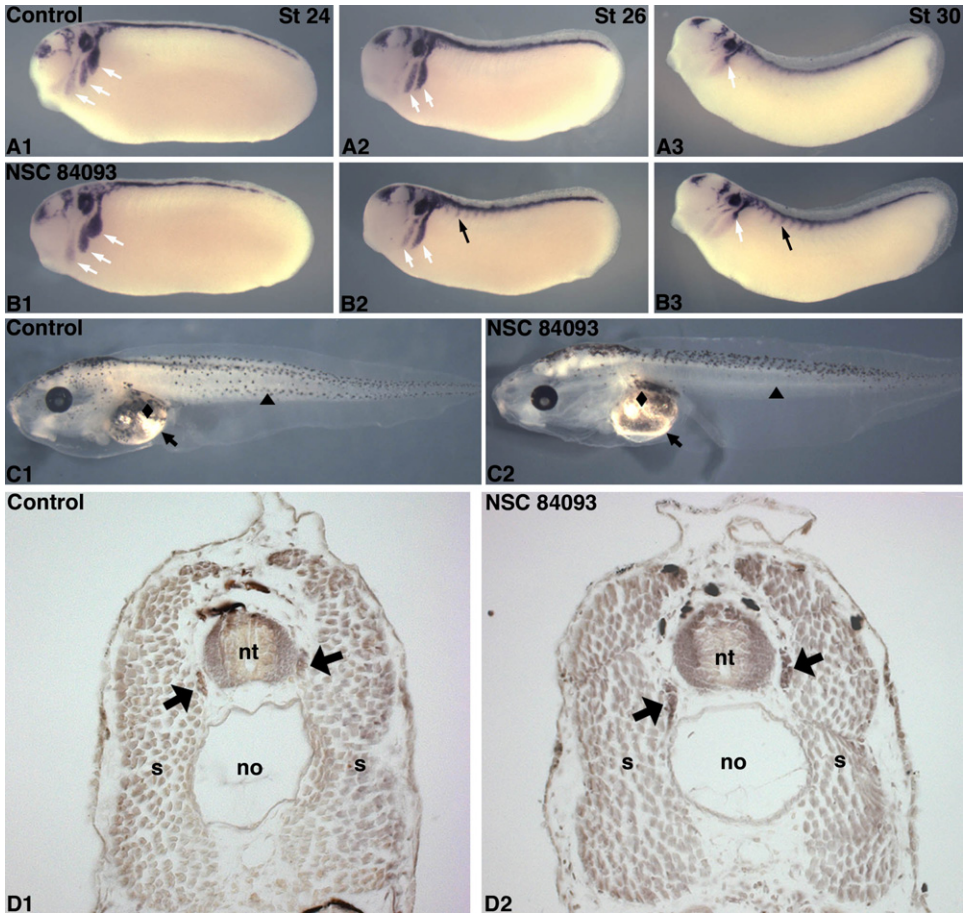

Figure 3. NSC 84093 Does Not Affect the Migration of Other NCC Derived Cells

(A and B) Effects on early cranial neural crest migration with the application of NSC 84093 using the molecular marker SOX-10. A1–3 shows the migration of cranial neural crest cells in untreated control embryos. B1–3 shows SOX-10 expression in embryos treated with 40 μM NSC 84093. A1 and B1 show stage 24, A2 and B2 are stage 26, and A3 and B3 are stage 30. Black arrows show the early segmented migration of trunk NCC in NSC 84093-treated embryos. White arrows indicate the migration of cranial NCC.

(C) Effects of NSC 84093 on the migration of trunk NCC-derived iridophores. C1 shows an untreated control embryo with the normal iridophore (iridescent gold to copper pigmented cells) position on the developing intestine (black arrow). C2 shows a NSC 84093-treated embryo with the segmented pattern of melanophores on the dorsal side of the embryo, where iridophores have migrated normally (black arrow). Both embryos are at stage 48, after iridophore migration. Diamond (◆) represents the lateral pigment stripe; arrowhead (▲) represents the dorsal pigment stripe.

(D) Effects of NSC 84093 on the migration of trunk NCC-derived dorsal root ganglion (DRG) cells. DRG cells are visualized with the neural specific antibody β-tubulin III and DAB staining. Transverse sections are shown at a point in the mid trunk section. D1 shows the normal migration of DRG cells between the somites and the neural tube in an untreated control embryo. D2 shows the migration of DRG cells in 40 μM NSC 84093-treated embryos. Black arrows indicate the stained DRG cells. Both embryos are at stage 48. n represents the notochord, nt shows the neural tube, s represents the somite. All embryos are shown in lateral view, with anterior to the left.

rescue the phenotype seen in treated embryos. The addition of manganese ions, magnesium ions, calcium ions, or ferrous iron with 1 μM NSC 84093 did not rescue the segmented pattern seen with the application of NSC 84093 (Figure 4, B1–B5). Ferrous iron did partially rescue the migration of melanophores to the tail.

Only the addition of zinc ions was able to restore the complete normal melanophore migration pattern (Figure 4, B6). The lowest concentration of zinc ions that was able to rescue migration was 30 nM (data not shown). The ability of both quinolin-8-ol and NSC 84093 to complex with zinc ions was further confirmed using in vitro titration assays (Figure S4). Ferrous iron can complex with both quinolin-8-ol and NSC 84093, but somewhat higher concentrations of ferrous iron are needed to achieve 50% complexation compared with zinc (data not shown). It has been shown that other MMP inhibitors can inhibit heme enzymes, suggesting an interaction with Fe (Jacobsen et al., 2008). Importantly, when zinc ions were added to the embryo buffer after the application of the compound, the phenotype could not be rescued (data not shown). This strongly suggests that the compound is not simply sequestering zinc ions away from the developing embryo, which is also supported by the lack of activity of the parent 8-hydroxyquinoline scaffold (Figure 4, A7).

Because MMPs are zinc-dependent enzymes and one of the potential molecular targets of NSC 84093, we set out to determine if NSC 84093 can inhibit MMPs. We previously reported the expression of MMP-14 in migrating neural crest cells

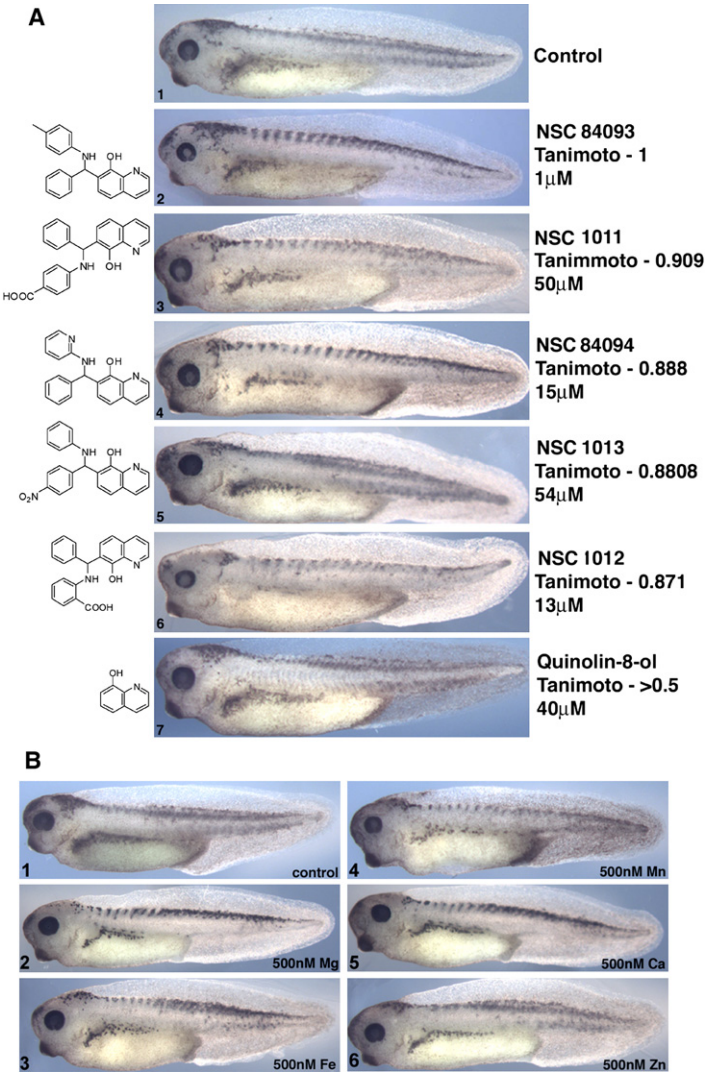

Figure 4. SAR Analysis and Ion Rescue Experiment of NSC 84093

(A) A series of analogs and compounds showing similar phenotypes to NSC 84093, ranked by pairwise Tanimoto coefficient scores. The dose tested is shown in μM. Dose-response curves have been done for all (Figure S1 for NSC 84093 and data not shown). Quinoline-8-ol is the scaffold compound used to synthesize the derivative compounds.

(B) Ion rescue experiment where embryos were treated with various ions at 500 nM and NSC 84093 at 1 μM. Note the embryo treated with zinc shows a rescue of the migration phenotype compared with the others. All embryos are shown in lateral view, with anterior to the left.

(Harrison et al., 2004). We have not identified any other MMPs expressed in the neural crest. MMP-2 showed expression at the same stages as MMP-14, but in tissues of the embryo that surround the migrating front of MMP-14 expressing neural crest cells (Figures 5A and 5B). MMP-2 was first seen to be expressed at stage 24 in the head mesenchyme (Figure 5, B1); at stage 26, expression was seen in the head mesenchyme and presomitic mesoderm (Figure 5, B2). In stage 30 embryos, MMP-2 showed localization to both head and trunk mesenchyme (Figure 5, B3). These are coincident with areas into which anterior and trunk NCC will migrate. By stage 34, expression was seen throughout the head, in the lateral mesoderm, and surrounding the somites (Figure 5, B4), as confirmed by sectioning (data not shown). Reverse-transcriptase polymerase chain reaction (PCR) analysis confirmed that expression of MMP-14 started just before MMP-2 (Figure 5C). TIMP-2 expression, which is thought to be necessary for MMP-14-mediated activation of MMP-2 (Kinoshita et al., 1998), starts at the same time as MMP-2 and at the same relative level of expression (Figure 5C).

To examine whether NSC 84093 could inhibit *Xenopus* MMP-2 activity, gelatin zymography was employed (Leber and Balkwill, 1997). We prepared stage 38 embryo lysates and saw a dose-dependent effect of NSC 84093 on *Xenopus* MMP-2 activity (Figure 6, A1). MMP-14 is a collagenase, and therefore is not amenable to gelatin zymography and could not be tested. One of the advantages of chemical genomics is the ability to transfer compounds to other species. To investigate if NSC 84093 was able to act as an MMP inhibitor of human MMPs, we assayed recombinant human MMP-2. Not only did NSC 84093 inhibit human MMP-2 activity, but it also showed a stronger level of inhibition than in *Xenopus* embryo lysate zymograms (Figure 6, A2).

NSC 84093 Demonstrates, In Silico, the Properties of an MMP Inhibitor

To confirm that NSC 84093 can act as a putative MMP inhibitor, we used an in silico docking approach. The potential binding sites and efficiency of binding of NSC 84093 to various MMPs was assessed. A range of human MMP catalytic domains was chosen for these analyses, as well as bovine carboxypeptidase A (Rees et al., 1983), which is not a member of the MMP family but is a zinc-dependent protease. As a control, two known MMP inhibitors, Batimastat and BBH, were also extracted from the Protein Data Bank (PDB) files, set up for AutoDock, and docked into the MMP structures. The ligand NSC 84093 could be docked successfully in all cases to give reasonable chemistry and binding energies that on average were 1.51 Kcal/mol lower than Batimastat and 0.90 Kcal/mol lower than BBH. Batimastat, BBH, and NSC 84093 are all projected to have weaker binding to the negative control bovine carboxypeptidase A. Crystal structures of the *Xenopus* MMPs are currently unavailable, which thus prevented their investigation. Batimastat and BBH were tested on developing *Xenopus* embryos and were found to either exert no effect or to give nonspecific effects, possibly due to problems of penetration into the embryo (data not shown). To investigate the potential binding modes of the ligand NSC 84093 to MMPs, MMP-14 was chosen because it was a potential target for NSC 84093. The ligand NSC 84093 was selected from the AutoDock NCI diversity set and prepared for docking to the MMP-14 structure (1BBQ) using a variety of procedures (see Experimental Procedures). Although the relative rankings between the different docking experiments were different, the

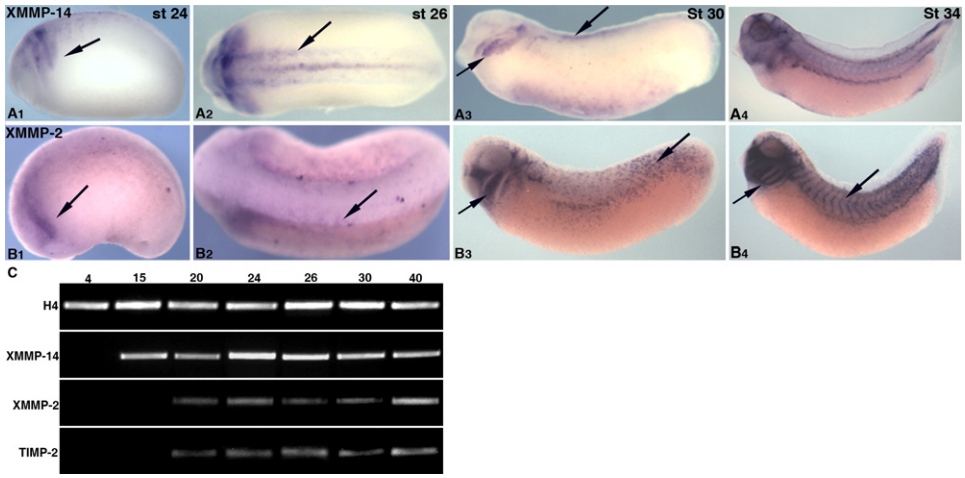

Figure 5. Expression Patterns of MMP-14 and MMP-2 in the Developing Embryo

MMP-14, previously reported in Harrison et al. (2004): (A1) stage 24, (A2) stage 26, (A3) stage 30, (A4) stage 34. MMP-2: (B1) stage 24, (B2) stage 26, (B3) stage 30, (B4) stage 34.

(C) The temporal expression pattern of MMP-14, MMP-2, and TIMP-2 during early *Xenopus* embryogenesis. Semiquantitative reverse transcriptase PCR analysis shows that MMP-14 expression is strong from stage 15 onward. MMP-2 and TIMP-2 expression is first seen from stage 20 onward. Arrows show areas of expression. All embryos are shown in lateral view, with anterior to the left.

observed top binding modes were highly similar. The interactions were those observed in Figure 6 (B1), in which we have drawn the zinc binding atom bonds in a dashed yellow line. Using the optimized Zn parameters, we obtain ligand-metal ion distances between the O and Zn of 1.92 Å and between N and Zn 1.90 Å in the top solution. The second-best solution has a distance of 1.7 Å between the O and Zn (Figure 6, B2). These other parameter sets introduce variation of these distances up to 2.8 Å for the O and 2.7 Å for N in the top docking solutions. In all cases, the ligand fits snugly into the binding pocket and with reasonable coordination geometry. These in silico results were confirmed by the in vitro titration assay, which confirms that the quinolin-8-ol scaffold compound acts as the zinc binding group of NSC 84093.

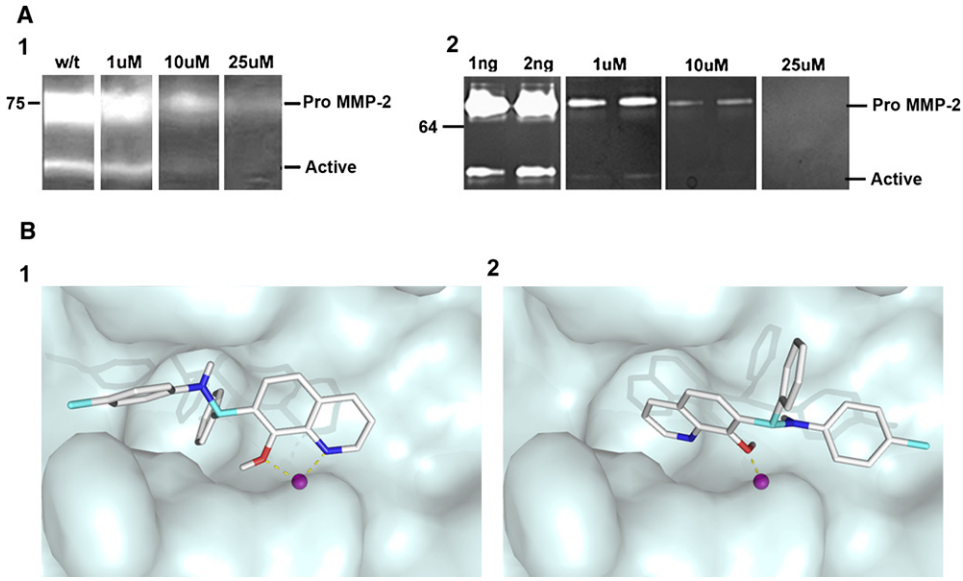

Figure 6. Gelatin Zymography of NSC 84093 on both *Xenopus* and Human MMP-2

(A1) Stage 38 embryo lysates (one embryo per lane), with stated concentrations of NSC 84093.

(A2) Recombinant human MMP-2 (1 and 2 ng) with stated concentrations of NSC 84093. Zymograms show both latent and activated MMP states.

(B) The top two binding modes of NSC 84093 to the M chain of 1BQQ, predicted by AutoDock using the optimized Zn parameters suggested by Hu and Shelver (2003). The Zn ion in shown in magenta. In B1 the distance between the O and Zn is 1.92 A, and between N and Zn 1.90 A, and the free binding energy was −10.1 kcal/mol. In B2 the O Zn distance is 1.7 A and the energy of free binding −9.8 kcal/mol.

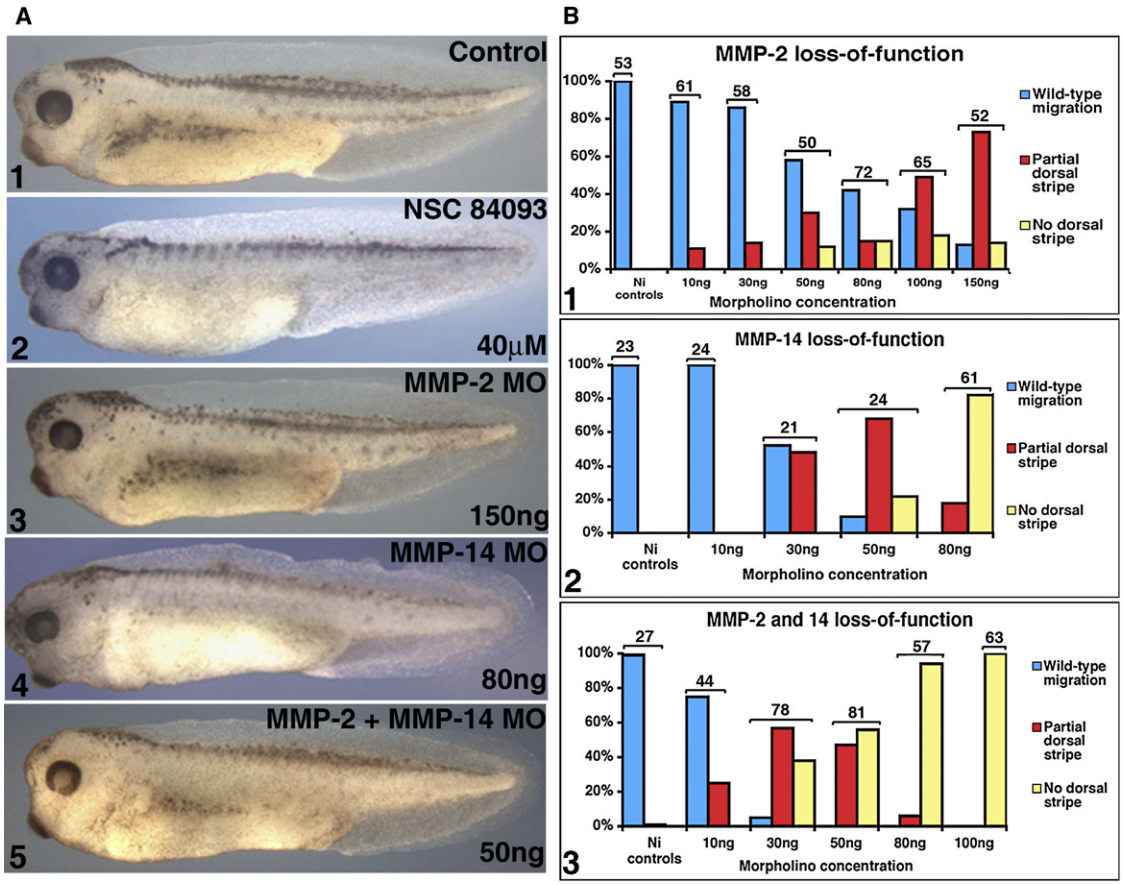

Figure 7. Dose-Dependent Effect on Melanophore Migration Seen with Increasing Concentrations of MMP-2 and MMP-14 MO

All embryos are stage 38. (A1) Control embryo, (A2) embryo treated from stage 15 onward with 40 μM NSC 84093, (A3) embryo injected with 150 ng MMP-2 MO, (A4) embryo injected with 50 ng MMP-14 MO, (A5) embryo injected with 30 ng each of MMP-2 and MMP-14 MO. (B1–3) Graphs showing the effects of increasing concentrations of MO on melanophore migration. (B1) MMP-2, (B2) MMP-14, and (B3) MMP-2 and MMP-14 injected together. Numbers above the bars correspond to the number of embryos injected. All embryos are shown in lateral view, with anterior to the left.

A Reduction in MMP-14 Leads to Inhibition of Melanophore Migration

It is known that MMP-2 can be activated by MMP-14 (Kinoshita et al., 1998), and it has been proposed that this is also the case in *Xenopus* (Hasebe et al., 2007). To investigate the function of MMP-2 and MMP-14 individually and in combination, specific antisense MOs were injected into the animal pole area of both blastomeres of 2-cell-stage embryos to ensure delivery to the neural tissues. In vitro translation experiments showed that the MMP-2 MO and MMP-14 MO were functional and dose dependent (Figure S3). A scrambled sequence MO (CMO) was used as a control in both embryos and in vitro translation assays. A dose-dependent inhibition of melanophore migration was seen with a serial dose of MMP-14 MO (Figure 7, A4 and B2). Injection of MMP-14 MO causes a partial, and at higher concentrations complete, loss of the dorsal and lateral stripes (Figure 7, B2). A weaker dose-dependent inhibition of melanophore migration was seen with increasing amounts of MMP-2 MO (Figure 7, A3 and B1). MMP-2 MO leads to a decrease in melanophores only on the ventral side of the tail. Coinjection of MMP-2 and MMP-14 MOs gives an effect similar to the MMP-14 MOs, but at lower concentrations (Figure 7, A5 and B3), suggesting that the two work in tandem to mediate melanophore migration. The MMP-14 and MMP-2 MOs did not at any point give the segmented phenotype seen in NSC 84093-treated embryos. These results were confirmed using in situ hybridization with the probe *XIDCT* at stage 32 (data not shown). Inhibition of the lateral pigment stripe was seen at stage 32 with high doses of MMP-2 MO. The relevant numbers of MO loss-of-function and control embryos showing the extent of migration are shown in Figure 7B. In the control embryo, pigment can clearly be seen in the dorsal and lateral stripes (Figure 7, A1).

DISCUSSION

Chemical Genomics Identifies a Putative Novel MMP Inhibitor

NSC 84093 was identified in a forward chemical genomic screen as affecting melanophore migration in developing *Xenopus laevis* embryos. It has not previously been reported to have an effect on cell migration. The segmented pigment phenotype (Figure 1D), to the best of our knowledge, has also not been previously observed. Using application of NSC 84093, we show an early segmental arrangement of the trunk *XIDCT*+ melanoblasts

(melanoblasts precede the more differentiated melanophores) (Figure S2). This pattern gives rise to the later segmented dorsal pattern (Figure 1D). Melanoblasts migrate between the neural tube and the somite, but then stop and do not continue to migrate either ventrally and/or caudally. Evidence of *Xenopus* neural crest cells primarily located to the midpoint of the somite has been reported (Collazo et al., 1993; Krotoski et al., 1988). NSC 84093 seems to act mainly on melanophores because neural crest derivatives such as cranial neural crest, iridophores, and the dorsal root ganglia are not affected. However, this does not rule out the possibility that other neural crests are also affected, especially because *SOX10* expression in NSC 84093-treated embryos also shows the characteristic segmented pattern.

The other aspect of the NSC 84093 phenotype is a lack of ventral tail melanophores. The segmented pattern and the inhibition of ventral tail melanophore migration could be caused by NSC 84093, inhibiting different molecular targets. Alternatively, they could be the consequence of the same event; for example, if 84093's target changes the adhesion properties on the somite surface, this would cause the melanophores to become restricted, a segmented pattern would arise, and the melanophores would be prevented from moving to the ventral side of the tail. Melanophores are observed on the somite surface, as seen in Figure 1. The somite surface is known to be extracellular matrix (ECM) rich (Allenspach and Clark, 1988). Somites have developed at this early stage (St 26), when melanoblasts have arisen. It has been proposed that cell migration is dependent on adhesivity, with migration proceeding at its fastest rate when adhesion is neither too strong nor too weak (Schwartz and Horwitz, 2006). Therefore, changes in adhesion between the melanoblasts and somites due to the compound could have the effect of stopping migration. The segmented and ventral tail phenotypes might thus be distinct biological events but caused by inhibiting the same molecular target or distinct events by different target proteins. Further investigation will be needed to clarify this situation.

The segmented pigment stripe of the NSC 84093 embryos treated at low concentrations (Figures 1D and 1F and Figure S1) was not seen with MMP-2 or MMP-14 morphant embryos on their own or in combination. However, at higher concentrations of NSC 84093, the segmented pattern was gradually lost in favor of a complete block in migration (Figure S1, panel 4), which is very similar to the effect of MO knockdown of MMP-14 at 80 ng and MMP-14 and MMP-2 together at 50 ng (compare Figure 7, A4 and A5, and Figure S1, panel 4). From our loss-of-function assays with MMP-2, it seemed that MMP-2 only affects the migration of melanophores to the ventral side of the tail when assayed at stage 38. This is most easily explained by melanophores migrating in an anterior-posterior wave. MMP-2 loss-of-function only delays their migration, so the ventral stripe is formed last. An alternative is the morpholino is diluted during growth of the embryo and its effect is lost with embryo development. Indeed when stage 32 embryos are investigated, lateral stripe melanophore migration was inhibited, although again higher concentrations are needed than with the MMP-14 MO whereas by stage 38 the lateral stripe appears normal (data not shown).

Through the application of NSC 84093 (Figure 1) and the MMP-2 and MMP-14 knockdown assays (Figure 7), we demonstrate that the ventral tail melanophores of the dorsal pigment stripe progress ventrally, down the tail of the embryo, on the somite surface. This can clearly be seen in Figure 2H (arrow). They do not seem to circumnavigate the tail as previously suggested (Collazo et al., 1993).

At higher concentrations, NSC 84093 might inhibit metalloproteinases more broadly as seen with MMP-2 and MMP-14, leading to a complete block in melanophore migration. MMP inhibitors tend to be broad spectrum in the enzymes they bind to and thus exert their effect to a differing degree across the whole family of MMPs, and indeed ADAMs (*A disintegrin and metalloproteinase* domain) and ADAMTS (*A disintegrin and metalloproteinase* domain with *thrombospondin* domains) enzymes as well (Agrawal et al., 2008; Jacobsen et al., 2007).

We speculate that at lower concentrations, NSC 84093 is potentially inhibiting a specific metalloproteinase. This could include an MMP or an ADAM or ADAMTS. There are other zinc-dependent proteins present in the embryos at this time and many proteins use zinc as a cofactor (Anzellotti and Farrell, 2008). However, given the evidence for MMP inhibition at high concentrations combined with the in silico data presented, we believe an MMP is the most likely target. Further investigation will need to be undertaken to ascertain the low concentration target of NSC 84093. At higher concentrations, NSC 84093 could be inhibiting a broader spectrum of metalloproteinases including MMP-14 and/or MMP-2. NSC 84093 still shows some specificity even at higher concentrations because it does not affect the migration of embryonic macrophages, which we have shown are dependent upon the function of MMP-7, MMP-9, and MMP-18 (Tomlinson et al., 2008 and data not shown).

There has been progress in identifying, and in some cases functionally characterizing, the various metalloproteinases expressed in the trunk region of the *Xenopus* embryo during NCC migration. Such proteins are possible candidates for the target of NSC 84093 at low concentrations. These include two members of the Tolloid-like family of metalloproteases, Xolloid-related (Xlr) (Dale et al., 2002) and BMP-1 (Goodman et al., 1998); ADAMs such as ADAM13, Xmdc9, and 11a (Alfandari et al., 1997; Cai et al., 1998); and ADAMTS1 (Suga et al., 2006). In the mouse, MMP-8 is expressed in migrating NCCs (Giambernardi et al., 2001). *Xenopus* MMP-8 has yet to be identified.

From our zinc ion rescue (Figure 4, B6), in silico docking experiments (Figure 6B), and titration assays (Figure S4), we conclude that the phenolic component of NSC 84093 is at least partly acting as a zinc-binding group, possibly in conjunction with the neighboring secondary amine as shown by the docking experiments (shown in Figure 6B). The branched structure of the compound (shown in Figure 1B) and the docking experiments indicate that the side chains of NSC 84093 are able to interact with the subsite pockets of the catalytic domain of MMPs (Figure 6B). The MMP's active site consists of six loosely defined subsites, three of which are located on either side of the catalytic zinc ion (Jacobsen et al., 2007). It seems clear that the side chains of NSC 84093 could occupy these pockets in silico and therefore inhibit enzyme activity. However, it might also be the case that the zinc binding site provides specificity of interaction as well (Agrawal et al., 2008). Docking NSC 84093 with bovine carboxypeptidase A suggests that NSC 84093 is probably not a promiscuous inhibitor of zinc-dependent enzymes, although

this possibility cannot rule out interactions with other zinc-dependent proteins. In vivo, a number of similar compounds based on the 8-quinolinol scaffold, as judged by Tanimoto scores, also had an effect on melanophore migration except for NSC 1013 (Figure 3A). It might be that the nitro group of NSC 1013, which might be reduced in vivo, binds to a different protein and/or is sequestered away from the melanophores. The 8-quinolinol scaffold and branched structures of these compounds appear critical for their phenotypic effect.

In the human MMP-2 zymograms, NSC 84093 showed a high level of inhibition of MMP-2 activity, again in a dose-dependent fashion (Figure 6, A2), as with the *Xenopus* MMP-2 zymograms (Figure 6, A1). These results further establish that NSC 84093 can act as an MMP inhibitor. The increased inhibition levels seen in the human MMP-2 zymograms compared with the *Xenopus* MMP-2 zymograms could be due to many factors, including the heterogeneity of an embryo lysate and the evolutionary divergence between human and *Xenopus* MMPs.

MMP-14 and MMP-2 Are Required for Melanophore Migration

Human MMP-14 was the first membrane-bound MMP to be identified (Puente et al., 1996) and was subsequently shown to be a specific activator of pro-MMP-2 (Sato et al., 1996). This MMP has received a great deal of attention due to its important function in the progression of malignant tumors (Sato et al., 2005). MMP-14 functions in cancer progression, both by the activation of pro-MMP-2 (Itoh et al., 2001) and by modification of the ECM type I collagen and other substrates (d'Ortho et al., 1997). The main basement membrane target of MMP-2 is type IV collagen (Hornebeck et al., 2002; Itoh et al., 2001). The mouse knockout of MMP-14 gives a severe phenotype, including problems in craniofacial development, dwarfism, and skeletal and extraskeletal connective tissue abnormalities (Holmbeck et al., 1999). The importance of MMP-14 and MMP-2 is emphasized by the fact that cancer cells proliferate within an embedded dense three-dimensional matrix that is composed largely of type I collagen. To metastasize they need to modify this matrix (Sato et al., 2005). Their expression patterns reflect these functions, with MMP-14 expressed on the leading edge of metastatic cancer cells acting as an invasion-promoting protease (Seiki et al., 2003), and MMP-2 localized in the stromal cells surrounding the tumor (Poulsom et al., 1992). Expression levels of MMP-14 have been closely associated with tumor invasiveness (Sato et al., 2005).

It has been shown that MMP-14 complexes with the endogenous MMP inhibitor TIMP-2 to activate MMP-2 (Itoh et al., 2001). The same interaction has been proposed to occur during *Xenopus* metamorphosis (Walsh et al., 2007). The temporal and spatial expression of MMP-2, MMP-14, and TIMP-2 in early *Xenopus* embryogenesis (Figure 5) suggests a similar mechanism occurring in the early frog embryo. MMP-14 expression on the migrating melanophores and MMP-2 expression in the surrounding mesenchyme along with the MO knockdowns (Figure 7) demonstrate that they both play a functional role in promoting the migration of melanophores in the developing *Xenopus* embryo. We speculate that in combination with TIMP2, MMP-14 is likely to be cleaving pro-MMP-2 in the encapsulating tissues, which in turn would be able to modify the surrounding ECM for the subsequent melanophore migration. Similar expression patterns for MMP-2 are seen in chick embryos at comparable stages in development, with MMP-2 being deposited by the mesenchymal cells (Cai et al., 2000; Duong and Erickson, 2004).

Despite the potential of chemical genomics, one of the biggest challenges to this new and emerging field is that of target identification. Although significant advances have been made in this area (Boshoff and Dowd, 2007; Burdine and Kodadek, 2004; Jung et al., 2005; Mitsopoulos et al., 2004), as yet there is no reliable and general method to identify the molecular target of a compound of interest. However, it is still feasible to narrow the range of potential molecular targets that need to be investigated for a novel bioactive compound (Luesch, 2006; Parsons et al., 2006). Here we present several approaches that could be transferable to other investigations of small, biologically active compounds. These include in silico docking experiments, an approach that is becoming increasingly important in structure-based drug design (Kitchen et al., 2004; Orry et al., 2006) and has the potential to play a further part in chemical genomic investigations (Figure 6B), an in vitro biochemical assay (Figure 6A), and the use of competition or rescue experiments (Figure 4B), which could be expanded to enzyme substrates or other candidate interactors.

SIGNIFICANCE

This study illustrates some of the advantages of a chemical genomic approach to investigate developmental processes, especially when used with complementary loss-of-function experiments. We identified NSC 84093 from a forward chemical genomic screen targeting melanophore (pigment cell) phenotypes and show it to be capable of acting as an MMP inhibitor. Fine temporal intervention in combination with other assays presented here has allowed us to show that NSC 84093's molecular target(s) act early in melanophore development to generate a segmented phenotype and slightly later to inhibit melanophore migration into the ventral tail region. Other neural crest derivatives are hard to distinguish, but we do not see any effects on cranial neural crest, iridophores, and development of the dorsal root ganglia. As such NSC 84093 provides us with a unique molecular tool to investigate melanophore migration. In addition, MO (antisense oligonucleotide) knockdown studies on MMP-14 and MMP-2 illustrate that MMPs play an essential role in melanophore migration during development and could be potential targets of NSC 84093. These results not only have implications in the context of developmental biology, but also have significance in understanding NCC migration and the roles of MMPs in the processes of cellular migration.

EXPERIMENTAL PROCEDURES

All experiments were performed in compliance with the relevant laws and institutional guidelines at the University of East Anglia. The research has been approved by the local ethical review committee according to UK Home Office regulations.

In Vitro and MO Assays

Xenopus embryos were obtained as previously described (Harrison et al., 2004). MO antisense oligonucleotides were microinjected into the two animal poles

of a 4-cell stage embryo, in serial dose experiments. MOs were designed by Gene tools based on supplied GenBank sequences (MMP-14 accession number AY6333953, MMP-2 accession number NM-001087228). The MMP-14 MO sequence is (5′-CCAGGCTGCTCTCAGAGGCTCCATC-3′). MMP-2 morpholino sequence is (5′ -CATGCTAAAGCCTGACTTTCTGCCG−3′). The scrambled sequence control morpholino (CMO) sequence is (5′-CCTCTTACC TCAGTTACAATTTATA−3′) MOs were subjected to in vitro translation assay before use (TNT coupled reticulocyte system, Promega), according to previously published methods (Abu-Elmagd et al., 2006).

In Situ Hybridization and Histology

MMP-2 in situ probes were generated from a MMP-2 pGEM clone. Briefly, primers were designed at the start and stop of PCRT7_GelAwtFLAG (Hasebe et al., 2007). Primer sequences are as follows: MMP-2 F (5′-CACCATGCGGA CAATTA-3′), MMP-2 R (5′-GCTACGCTGCGACTACAAG-3′). A standard PCR protocol was followed using Pfu polymerase (Promega) for its high fidelity. We performed 30 amplification cycles with a 55°C annealing and a 72°C extension temperature, and a final 72°C 10 min incubation with 1 μl of Taq polymerase (Invitrogen) was done to add A residues for the subsequent TOPO cloning step. The purified PCR product was then ligated into PGem-T Easy (Promega). Clones were then validated by DNA sequencing. Whole-mount in situ hybridization assays were done as previously described (Harrison et al., 2004). Paraffin wax sectioning was done to examine internal melanophore localization according to previously published methods (Harrison et al., 2004).

Immunohistochemistry

Immunohistochemistry was performed on stage 48 embryos to visualize the dorsal root ganglion cells. Embryos were fixed overnight in Dents fix (4:1 methanol:DMSO) and permeabilized in phosphate-buffered saline (PBS) containing 0.5% Triton X-100 and a 10 min proteinase K digestion and blocked with 2% Boehringer Blocking Reagent (Roche). Primary antibodies used were β-tubulin III (Sigma T2200, 1:100). Diaminobenzidine tetrahydrochloride (DAB) staining was achieved with a 2:1 solution of DAB and nickel chloride in PBS containing 0.5% Triton X-100. Paraffin sections prepared as outlined above.

Compound Application

NSC 84093 was identified in a screen of 3000 compounds looking for inhibitors of pigment patterning during *Xenopus* development. NSC 84093 and other compounds used in the study were obtained from the Diversity set, National Cancer Institute (NCI), and prepared as 10 mM stock solutions in dimethyl sulfoxide. The embryos were arrayed by Pasteur pipette, 10 embryos per 5 cm Petri dish containing 10 ml of 0.1XMMR (Marcs modified ringers, respectively, supplemented with 50 μg/ml gentamycin sulfate). Embryos were grown at 18°C, staged according to previously published criteria (Nieuwkoop and Faber, 1994), and photographed using previously published methods (Harrison et al., 2004).

Metal Ion Rescue Experiments

Coaddition of various ions at 500 nM included manganese ions ($MnCl_2$), magnesium ions ($MgCl_2$), calcium ions ($CaCl_2$), zinc ions ($ZnSO_4$), and ferrous iron citrate ($C_6H_5FeO_7$) with the application of the NSC 84093 compound at 1 μM. Assays performed with 10 embryos per 5 cm Petri dish containing 10 ml 0.1XMMR, supplemented with 50 μg/ml gentamycin sulfate.

In Vitro Zinc Titration Assays

The wavelength of maximum absorption change was determined by titrating a 1 mM MeOH solution of quinolin-8-ol or NSC 84093 (500 μl in a 1 ml glass cuvette) with 20 mM aqueous $ZnSO_4$ in 1 μl steps and acquiring UV/VIS spectrum on a Perkin Elmer Lambda 25 UV/VIS spectrometer. This maximum was determined to be 405 nm (for NSC 84093) and 375 nm (for quinolin-8-ol). The titration curves for quinolin-8-ol and NSC 84093 were determined using a multiwell plate reader (Dynex MRX^{TC} Revelation) at A_{405}. The final concentration in each well (total volume 100 μl) of quinolin-8-ol and NSC 84093 (methanolic stocks) was 100 μM. The final concentration of zinc ions (aqueous stocks) were decreasing by a factor of 10 starting with 100 mM down to 1 nM.

Tanimoto Pairwise Coefficient Analysis

To allow a pairwise comparison and ranking of analogs of compound NSC 84093, a web-based Tanimoto algorithm was used, calculated by using the Chembank website (http://chembank.broad.harvard.edu/) and the Daylight fingerprint algorithm. SMILES (Simplified Molecular Input Line Entry Specification) of the compound under investigation were obtained from the NCI website (http://dtp.nci.nih.gov/docs/dtp_search.html) and used to perform a similarity search on the Chembank website (http://chembank.broad.harvard.edu/), with the following variables defined: Tanimoto similarity metric and a similarity threshold (distance) of 0.8.

Gelatin Zymography

Stage 38 embryo lysates were dissected before lysis to exclude the head region and the yolk area. Human recombinant MMP-2 was obtained from R&D systems (902-MP). Gelatin zymography was done as previously described (Leber and Balkwill, 1997). Both embryo lysates and recombinant MMP-2 were activated before being assayed. Activation was achieved by adding 4-aminophenylmercuric acetate (A9563) to a 1 mM final concentration and incubating at 37°C for 1 hr.

In Silico Docking Experiments

MMP structures (3AYK, 1QIB, 2DIO, 1BZS, 1MMP, 1UTT, 1RM8, 1BBQ, and 5CPA) were downloaded from the PDB and prepared for AutoDock 3.0 using the AutoDockTools graphical interface. Hydrogens and Kollman charges were added. The Zn^{2+} charge was set to a value of +0.95 as suggested by Hu and Shelver based on their zinc binding group optimization study (Hu and Shelver, 2003). Autodock 3.0 does not have Zn parameters, so the optimized parameters of Hu and Shelver were assigned (radius = 0.87 Å, well depth = 0.35 kcal/mol). The structure of NSC 84093 was taken from the NCI diversity set available in AutoDock format from the AutoDock website. A grid size of 62 × 62 × 62 was chosen with a grid spacing of 0.375 Å, which completely covers the binding pocket. The Lamarckian genetic algorithm was chosen as the optimizer with the default settings. As a control, two known MMP inhibitors, Batimastat and BBH, were also extracted from PDB files, set up for AutoDock, and docked to the MMP structures.

To investigate the potential binding modes of the ligand NSC 84093 to MMP-14, the MMP structure 1BBQ was employed. The ligand NSC 84093 was selected from the AutoDock NCI diversity set and prepared for docking following the recommended procedure from the AutoDock manual. A grid size of 80 × 80 × 80 with a spacing of 0.225 Å, centered on the Zn atom of the binding pocket, was used to sample the interactions with the ligands. AutoDock 4.0 has Zn force field parameters, but we also experimented with the Stote and Karplus parameters (r = 1.1 Å, epsilon = 0.25 kcal/mol, q = +2) (Stote and Karplus, 1995) and the optimized parameters of Hu and Shelver (r = 087 Å, well depth = 0.35 kcal/mol, q = +0.95) (Hu and Shelver, 2003). We also tried deprotonating the ligand prior to docking. We chose a population size of 250, a function evaluation maximum of 25,000,000, and 30 runs, but otherwise stuck with the default docking parameters.

SUPPLEMENTAL DATA

The Supplemental Data include four figures and can be found with this article online at http://www.cell.com/chemistry-biology/supplemental/S1074-5521(08)00002-7.

ACKNOWLEDGMENTS

The *X1DCT* clone was a gift of H. Yamamoto (Department of Developmental Biology and Neurosciences, Tohoku University, Japan). MMP-2 and MMP-14 clones were donated by Y. B. Shi (National Institute of Child Health, NIH, Bethesda, MD, USA). We gratefully acknowledge the NCI/DTP Open Chemical Repository (http://dtp.nci.nih.gov) for supplying NSC 84093. We acknowledge helpful discussions with Jelena Gavrilovic, Dylan Edwards, Ian Clark, Andrea Munsterberg, Vincent Dive, and the rest of the Wheeler and Munsterberg labs. We thank Mohammed Hajihosseni for his help with the immunohistochemistry. M.T. was funded by the BBSRC and Pfizer through an Industrial CASE PhD studentship. C.G.M. was funded by a studentship from the Universidad Autonoma del Estado de Mexico. R.A.F. and G.N.W. also thank the UK

Medical Research Council for support through a Discipline Hopping award (grant no. G0100722).

Received: March 4, 2008
Revised: December 10, 2008
Accepted: December 12, 2008
Published: January 29, 2009

REFERENCES

Abu-Elmagd, M., Garcia-Morales, C., and Wheeler, G.N. (2006). Frizzled7 mediates canonical Wnt signaling in neural crest induction. Dev. Biol. *298*, 285–298.

Adams, D.S., and Levin, M. (2006). Inverse drug screens: a rapid and inexpensive method for implicating molecular targets. Genesis *44*, 530–540.

Agrawal, A., Romero-Perez, D., Jacobsen, J.A., Villarreal, F.J., and Cohen, S.M. (2008). Zinc-binding groups modulate selective inhibition of MMPs. ChemMedChem *3*, 812–820.

Alfandari, D., Wolfsberg, T.G., White, J.M., and DeSimone, D.W. (1997). ADAM 13: a novel ADAM expressed in somitic mesoderm and neural crest cells during *Xenopus laevis* development. Dev. Biol. *182*, 314–330.

Allenspach, A.L., and Clark, P.J. (1988). Retention and structure of extracellular matrix in early chick embryos after quick-freezing and freeze-substitution. Eur. J. Cell Biol. *46*, 531–538.

Anderson, C., Bartlett, S.J., Gansner, J.M., Wilson, D., He, L., Gitlin, J.D., Kelsh, R.N., and Dowden, J. (2007). Chemical genetics suggests a critical role for lysyl oxidase in zebrafish notochord morphogenesis. Mol. Biosyst. *3*, 51–59.

Ansari, A.Z. (2007). Chemical crosshairs on the central dogma. Nat. Chem. Biol. *3*, 2–7.

Anzellotti, A.I., and Farrell, N.P. (2008). Zinc metalloproteins as medicinal targets. Chem. Soc. Rev. *37*, 1629–1651.

Boshoff, H.I., and Dowd, C.S. (2007). Chemical genetics: an evolving toolbox for target identification and lead optimization. Prog. Drug Res. *64*, 51–77.

Burdine, L., and Kodadek, T. (2004). Target identification in chemical genetics: the (often) missing link. Chem. Biol. *11*, 593–597.

Burns, C.G., Milan, D.J., Grande, E.J., Rottbauer, W., MacRae, C.A., and Fishman, M.C. (2005). High-throughput assay for small molecules that modulate zebrafish embryonic heart rate. Nat. Chem. Biol. *1*, 263–264.

Cai, D.H., Vollberg, T.M., Sr., Hahn-Dantona, E., Quigley, J.P., and Brauer, P.R. (2000). MMP-2 expression during early avian cardiac and neural crest morphogenesis. Anat. Rec. *259*, 168–179.

Cai, H., Kratzschmar, J., Alfandari, D., Hunnicutt, G., and Blobel, C.P. (1998). Neural crest-specific and general expression of distinct metalloprotease-disintegrins in early *Xenopus laevis* development. Dev. Biol. *204*, 508–524.

Carroll, P.M., Dougherty, B., Ross-Macdonald, P., Browman, K., and FitzGerald, K. (2003). Model systems in drug discovery: chemical genetics meets genomics. Pharmacol. Ther. *99*, 183–220.

Collazo, A., Bronner-Fraser, M., and Fraser, S.E. (1993). Vital dye labelling of Xenopus laevis trunk neural crest cells reveals multipotency and novel pathways of migration. Development *118*, 363–376.

Cooper, M.K., Porter, J.A., Young, K.E., and Beachy, P.A. (1998). Teratogen-mediated inhibition of target tissue response to Shh signaling. Science *280*, 1603–1607.

d'Ortho, M.P., Will, H., Atkinson, S., Butler, G., Messent, A., Gavrilovic, J., Smith, B., Timpl, R., Zardi, L., and Murphy, G. (1997). Membrane-type matrix metalloproteinases 1 and 2 exhibit broad-spectrum proteolytic capacities comparable to many matrix metalloproteinases. Eur. J. Biochem. *250*, 751–757.

Dale, L., Evans, W., and Goodman, S.A. (2002). Xolloid-related: a novel BMP1/Tolloid-related metalloprotease is expressed during early *Xenopus* development. Mech. Dev. *119*, 177–190.

Ding, S., and Schultz, P.G. (2004). A role for chemistry in stem cell biology. Nat. Biotechnol. *22*, 833–840.

Duong, T.D., and Erickson, C.A. (2004). MMP-2 plays an essential role in producing epithelial-mesenchymal transformations in the avian embryo. Dev. Dyn. *229*, 42–53.

Eccles, S.A., Box, C., and Court, W. (2005). Cell migration/invasion assays and their application in cancer drug discovery. Biotechnol. Annu. Rev. *11*, 391–421.

Fukumoto, T., Kema, I.P., and Levin, M. (2005). Serotonin signaling is a very early step in patterning of the left-right axis in chick and frog embryos. Curr. Biol. *15*, 794–803.

Giambernardi, T.A., Sakaguchi, A.Y., Gluhak, J., Pavlin, D., Troyer, D.A., Das, G., Rodeck, U., and Klebe, R.J. (2001). Neutrophil collagenase (MMP-8) is expressed during early development in neural crest cells as well as in adult melanoma cells. Matrix Biol. *20*, 577–587.

Goodman, S.A., Albano, R., Wardle, F.C., Matthews, G., Tannahill, D., and Dale, L. (1998). BMP1-related metalloproteinases promote the development of ventral mesoderm in early *Xenopus* embryos. Dev. Biol. *195*, 144–157.

Haass, N.K., Smalley, K.S., Li, L., and Herlyn, M. (2005). Adhesion, migration and communication in melanocytes and melanoma. Pigment Cell Res. *18*, 150–159.

Harrison, M., Abu-Elmagd, M., Grocott, T., Yates, C., Gavrilovic, J., and Wheeler, G.N. (2004). Matrix metalloproteinase genes in *Xenopus* development. Dev. Dyn. *231*, 214–220.

Hasebe, T., Hartman, R., Fu, L., Amano, T., and Shi, Y.B. (2007). Evidence for a cooperative role of gelatinase A and membrane type-1 matrix metalloproteinase during *Xenopus laevis* development. Mech. Dev. *124*, 11–22.

Hofmann, U.B., Westphal, J.R., Van Muijen, G.N., and Ruiter, D.J. (2000). Matrix metalloproteinases in human melanoma. J. Invest. Dermatol. *115*, 337–344.

Holmbeck, K., Bianco, P., Caterina, J., Yamada, S., Kromer, M., Kuznetsov, S.A., Mankani, M., Robey, P.G., Poole, A.R., Pidoux, I., et al. (1999). MT1-MMP-deficient mice develop dwarfism, osteopenia, arthritis, and connective tissue disease due to inadequate collagen turnover. Cell *99*, 81–92.

Honore, S.M., Aybar, M.J., and Mayor, R. (2003). Sox10 is required for the early development of the prospective neural crest in *Xenopus* embryos. Dev. Biol. *260*, 79–96.

Hornebeck, W., Emonard, H., Monboisse, J.C., and Bellon, G. (2002). Matrix-directed regulation of pericellular proteolysis and tumor progression. Semin. Cancer Biol. *12*, 231–241.

Hruby, M., Hradil, J., and Benes, M. (2004). Interactions of phenols with silver(I), copper(II) and iron(II) complexes of chelating methacrylate-based polymeric sorbent containing quinolin-8-ol groups. React. Funct. Polymers *59*, 105–118.

Hu, X., and Shelver, W.H. (2003). Docking studies of matrix metalloproteinase inhibitors: zinc parameter optimization to improve the binding free energy prediction. J. Mol. Graph. Model. *22*, 115–126.

Itoh, Y., Takamura, A., Ito, N., Maru, Y., Sato, H., Suenaga, N., Aoki, T., and Seiki, M. (2001). Homophilic complex formation of MT1-MMP facilitates proMMP-2 activation on the cell surface and promotes tumor cell invasion. EMBO J. *20*, 4782–4793.

Jacobsen, F.E., Buczynski, M.W., Dennis, E.A., and Cohen, S.M. (2008). A macrophage cell model for selective metalloproteinase inhibitor design. ChemBioChem *9*, 2087–2095.

Jacobsen, F.E., Lewis, J.A., and Cohen, S.M. (2007). The design of inhibitors for medicinally relevant metalloproteins. ChemMedChem *2*, 152–171.

Jung, D., Williams, D., Kershonsky, S.M., Kang, T., Heidary, N., Chang, Y.T., and Orlow, S.J. (2005). Identification of the F1F0 mitochondrial ATPase as a target for modulating skin pigmentation by screening a tagged triazine library in zebrafish. Mol. Biosyst. *1*, 85–92.

Kinoshita, T., Sato, H., Okada, A., Ohuchi, E., Imai, K., Okada, Y., and Seiki, M. (1998). TIMP-2 promotes activation of progelatinase A by membrane-type 1 matrix metalloproteinase immobilized on agarose beads. J. Biol. Chem. *273*, 16098–16103.

Kitchen, D.B., Decornez, H., Furr, J.R., and Bajorath, J. (2004). Docking and scoring in virtual screening for drug discovery: methods and applications. Nat. Rev. Drug Discov. *3*, 935–949.

Knight, Z.A., and Shokat, K.M. (2007). Chemical genetics: where genetics and pharmacology meet. Cell *128*, 425–430.

Krotoski, D.M., Fraser, S.E., and Bronner-Fraser, M. (1988). Mapping of neural crest pathways in *Xenopus laevis* using inter- and intra-specific cell markers. Dev. Biol. *127*, 119–132.

Kumasaka, M., Sato, S., Yajima, I., and Yamamoto, H. (2003). Isolation and developmental expression of tyrosinase family genes in *Xenopus laevis*. Pigment Cell Res. *16*, 455–462.

Kwok, T.C., Ricker, N., Fraser, R., Chan, A.W., Burns, A., Stanley, E.F., McCourt, P., Cutler, S.R., and Roy, P.J. (2006). A small-molecule screen in C. elegans yields a new calcium channel antagonist. Nature *441*, 91–95.

Lamason, R.L., Mohideen, M.A., Mest, J.R., Wong, A.C., Norton, H.L., Aros, M.C., Jurynec, M.J., Mao, X., Humphreville, V.R., Humbert, J.E., et al. (2005). SLC24A5, a putative cation exchanger, affects pigmentation in zebrafish and humans. Science *310*, 1782–1786.

Langheinrich, U. (2003). Zebrafish: a new model on the pharmaceutical catwalk. Bioessays *25*, 904–912.

Langheinrich, U., Hennen, E., Stott, G., and Vacun, G. (2002). Zebrafish as a model organism for the identification and characterization of drugs and genes affecting p53 signaling. Curr. Biol. *12*, 2023–2028.

Le Douarin, N.M., and Dupin, E. (2003). Multipotentiality of the neural crest. Curr. Opin. Genet. Dev. *13*, 529–536.

Leber, T.M., and Balkwill, F.R. (1997). Zymography: a single-step staining method for quantitation of proteolytic activity on substrate gels. Anal. Biochem. *249*, 24–28.

Lin, G., Chen, Y., and Slack, J.M. (2007). Regeneration of neural crest derivatives in the *Xenopus* tadpole tail. BMC Dev. Biol. *7*, 56.

Luesch, H. (2006). Towards high-throughput characterization of small molecule mechanisms of action. Mol. Biosyst. *2*, 609–620.

Lunn, M.R., and Stockwell, B.R. (2005). Chemical genetics and orphan genetic diseases. Chem. Biol. *12*, 1063–1073.

Mathew, L.K., Sengupta, S., Kawakami, A., Andreasen, E.A., Lohr, C.V., Loynes, C.A., Renshaw, S.A., Peterson, R.T., and Tanguay, R.L. (2007). Unraveling tissue regeneration pathways using chemical genetics. J. Biol. Chem. *282*, 35202–35210.

Mitsopoulos, G., Walsh, D.P., and Chang, Y.T. (2004). Tagged library approach to chemical genomics and proteomics. Curr. Opin. Chem. Biol. *8*, 26–32.

Nieuwkoop, P.D., and Faber, J. (1994). Normal Table of *Xenopus laevis* (Daudin): A Systematical and Chronological Survey of the Development from the Fertilized Egg till the End of Metamorphosis (New York: Garland Publishing).

Orry, A.J., Abagyan, R.A., and Cavasotto, C.N. (2006). Structure-based development of target-specific compound libraries. Drug Discov. Today *11*, 261–266.

Parsons, A.B., Lopez, A., Givoni, I.E., Williams, D.E., Gray, C.A., Porter, J., Chua, G., Sopko, R., Brost, R.L., Ho, C.H., et al. (2006). Exploring the mode-of-action of bioactive compounds by chemical-genetic profiling in yeast. Cell *126*, 611–625.

Peterson, R.T., Link, B.A., Dowling, J.E., and Schreiber, S.L. (2000). Small molecule developmental screens reveal the logic and timing of vertebrate development. Proc. Natl. Acad. Sci. USA *97*, 12965–12969.

Peterson, R.T., Mably, J.D., Chen, J.N., and Fishman, M.C. (2001). Convergence of distinct pathways to heart patterning revealed by the small molecule concentramide and the mutation heart-and-soul. Curr. Biol. *11*, 1481–1491.

Poulsom, R., Pignatelli, M., Stetler-Stevenson, W.G., Liotta, L.A., Wright, P.A., Jeffery, R.E., Longcroft, J.M., Rogers, L., and Stamp, G.W. (1992). Stromal expression of 72 kda type IV collagenase (MMP-2) and TIMP-2 mRNAs in colorectal neoplasia. Am. J. Pathol. *141*, 389–396.

Puente, X.S., Pendas, A.M., Llano, E., Velasco, G., and Lopez-Otin, C. (1996). Molecular cloning of a novel membrane-type matrix metalloproteinase from a human breast carcinoma. Cancer Res. *56*, 944–949.

Rees, D.C., Lewis, M., and Lipscomb, W.N. (1983). Refined crystal structure of carboxypeptidase A at 1.54 A resolution. J. Mol. Biol. *168*, 367–387.

Riley, P.A. (1997). Melanin. Int. J. Biochem. Cell Biol. *29*, 1235–1239.

Sato, H., Takino, T., Kinoshita, T., Imai, K., Okada, Y., Stetler Stevenson, W.G., and Seiki, M. (1996). Cell surface binding and activation of gelatinase A induced by expression of membrane-type-1-matrix metalloproteinase (MT1-MMP). FEBS Lett. *385*, 238–240.

Sato, H., Takino, T., and Miyamori, H. (2005). Roles of membrane-type matrix metalloproteinase-1 in tumor invasion and metastasis. Cancer Sci. *96*, 212–217.

Schreiber, S.L. (1998). Chemical genetics resulting from a passion for synthetic organic chemistry. Bioorg. Med. Chem. *6*, 1127–1152.

Schwartz, M.A., and Horwitz, A.R. (2006). Integrating adhesion, protrusion, and contraction during cell migration. Cell *125*, 1223–1225.

Seiki, M., Mori, H., Kajita, M., Uekita, T., and Itoh, Y. (2003). Membrane-type 1 matrix metalloproteinase and cell migration. Biochem. Soc. Symp. *70*, 253–262.

Singh, R.J., Mason, J.C., Lidington, E.A., Edwards, D.R., Nuttall, R.K., Khokha, R., Knauper, V., Murphy, G., and Gavrilovic, J. (2005). Cytokine stimulated vascular cell adhesion molecule-1 (VCAM-1) ectodomain release is regulated by TIMP-3. Cardiovasc. Res. *67*, 39–49.

Spring, D.R. (2005). Chemical genetics to chemical genomics: small molecules offer big insights. Chem. Soc. Rev. *34*, 472–482.

Stockwell, B.R. (2000). Chemical genetics: ligand-based discovery of gene function. Nat. Rev. Genet. *1*, 116–125.

Stote, R.H., and Karplus, M. (1995). Zinc binding in proteins and solution: a simple but accurate nonbonded representation. Proteins *23*, 12–31.

Suga, A., Hikasa, H., and Taira, M. (2006). *Xenopus* ADAMTS1 negatively modulates FGF signaling independent of its metalloprotease activity. Dev. Biol. *295*, 26–39.

Tomlinson, M.L., Field, R.A., and Wheeler, G.N. (2005). *Xenopus* as a model organism in developmental chemical genetic screens. Mol. Biosyst. *1*, 223–228.

Tomlinson, M.L., Garcia-Morales, C., Abu-Elmagd, M., and Wheeler, G.N. (2008). Three matrix metalloproteinases are required in vivo for macrophage migration during embryonic development. Mech. Dev. *125*, 1059–1070.

Tomlinson, M.L., Fidock, M., Field, R.A., and Wheeler, G.N. (2009). A developmental chemical genomic screen in Xenopus. Mol. Biosyst., in press. 10.1039/B818695B.

Walsh, L.A., Carere, D.A., Cooper, C.A., and Damjanovski, S. (2007). Membrane type-1 matrix metalloproteinases and tissue inhibitor of metalloproteinases-2 RNA levels mimic each other during *Xenopus laevis* metamorphosis. PLoS ONE *2*, e1000.

Yang, C.T., and Johnson, S.L. (2006). Small molecule-induced ablation and subsequent regeneration of larval zebrafish melanocytes. Development *133*, 3563–3573.

Yang, C.T., Hindes, A.E., Hultman, K.A., and Johnson, S.L. (2007). Mutations in gfpt1 and skiv2l2 cause distinct stage-specific defects in larval melanocyte regeneration in zebrafish. PLoS Genet. *3*, e88.

Yeh, J.R., and Crews, C.M. (2003). Chemical genetics: adding to the developmental biology toolbox. Dev. Cell *5*, 11–19.

Yu, P.B., Hong, C.C., Sachidanandan, C., Babitt, J.L., Deng, D.Y., Hoyng, S.A., Lin, H.Y., Bloch, K.D., and Peterson, R.T. (2008). Dorsomorphin inhibits BMP signals required for embryogenesis and iron metabolism. Nat. Chem. Biol. *4*, 33–41.

Zon, L.I., and Peterson, R.T. (2005). In vivo drug discovery in the zebrafish. Nat. Rev. Drug Discov. *4*, 35–44.